Near Surface Geophysics

EAGE EUROPEAN ASSOCIATION OF GEOSCIENTISTS & ENGINEERS

Near Surface Geophysics, 2020, **18**, 427–443 doi: 10.1002/nsg.12110

Quantifying seasonal 3D effects for a permanent electrical resistivity tomography monitoring system along the embankment of an irrigation canal

Azadeh Hojat[1,2*], Diego Arosio[3], Vladislav Ivov Ivanov[1], Meng Heng Loke[4], Laura Longoni[1], Monica Papini[1], Greta Tresoldi[1] and Luigi Zanzi[1]

[1]*Dipartimento di Ingegneria Civile e Ambientale, Politecnico di Milano, Milan, 20133, Italy,* [2]*Department of Mining Engineering, Shahid Bahonar University of Kerman, Kerman, 76188, Iran,* [3]*Dipartimento di Scienze Chimiche e Geologiche, Università degli Studi di Modena e Reggio Emilia, Modena, 41125, Italy, and* [4]*Geotomo Software Sdn Bhd, Malaysia*

Received January 2020, revision accepted June 2020

ABSTRACT

In this paper, we discuss the necessity of quantifying and correcting seasonal 3D effects on 2D electrical resistivity tomography (ERT) data measured along the embankments of rivers or artificial canals. A permanent ERT monitoring system has been continuously operating along the levee of an irrigation canal in Mantua province, Italy, since September 2015. To evaluate the importance of 3D effects and their dependence on seasonal variations, we first performed numerical simulations and also laboratory tests on downscaled levees of the study site. The results showed that 2D apparent resistivity pseudosections measured along the levee are significantly affected by 3D effects of the embankment geometry. Moreover, it was observed that 3D effects not only depend on the levee geometry, but they are also affected by seasonal fluctuations in the water level in the canal. This proved the importance of calculating 3D effects for the study site during dry and irrigation periods. Therefore, different synthetic models based on the levee geometry and water level in the canal in each period were constructed in RES2DMOD and RES3DMODx64 to quantify 3D effects for the study site. The ratios of apparent resistivity values calculated in RES3DMODx64 to the values calculated in RES2DMOD showed that 3D effects approach a maximum of 30% when the canal is empty during winter, and they arrive at a maximum of 10% when the canal is filled with water in summer. Using the graphs of the modelled 3D effects as a function of electrode spacing, apparent resistivity pseudosections measured by the permanent ERT system are corrected for 3D effects to obtain reliable resistivity sections after inversion. The final resistivity maps can be then converted into water content images using the empirical and site-dependent relationship developed from core samples in the study area. Water content maps can be used to evaluate the stability of the levee and to detect possible seepage zones.

Key words: 2D inversion, 3D effects, Electrical resistivity tomography, River levee.

INTRODUCTION

Failure of earthen embankments can occur on the slopes of roadways and railways, earth dams and river levees. Improper design and construction procedure, insufficient compaction,

*E-mail: azadeh.hojat@polimi.it; ahojat@uk.ac.ir

seepage, overflow, breaching, erosion, extreme drying seasons and inadequate maintenance are some of the most common reasons of embankment failures. Devastating floods and excessive rainfalls can accelerate the failure of such embankments. An assessment of flood risk in Europe showed that the socio-economic impact of river floods, due to the climate change alone, would increase by an average of 220% by the end of the century (Alfieri *et al*., 2015). Therefore, there is an increasing need to develop efficient methods to monitor the internal hydrogeological conditions of river embankments.

Geophysical methods have been widely used to assess the stability of slopes and embankments (Dahlin *et al*., 2005; Godio *et al*., 2006; Chambers *et al*., 2009, 2014; Heincke *et al*., 2010; Supper *et al*., 2014; Arosio *et al*., 2017; Bièvre *et al*., 2018; Hojat *et al*., 2019a, c; Zhang *et al*., 2019). The electrical resistivity tomography (ERT) method has specifically been shown to be efficient in monitoring the variations of water saturation and detecting seepage zones for a variety of studies applied to hydrogeological issues (Piegari *et al*., 2008; Chambers at al. 2009, 2014; Kuras *et al*., 2009; Karimi-Nasab *et al*., 2011; Perrone *et al*., 2014; Supper *et al*., 2014; Arosio *et al*., 2017; Uhlemann *et al*., 2017; Whiteley, Chambers Uhlemann, 2017; Tresoldi *et al*., 2018, 2019; Hojat *et al*., 2019a,c,d). The main purpose of such measurements is to develop real-time monitoring systems capable of highlighting the internal heterogeneities of the embankments at the time they start to develop in order to promptly plan mitigation actions.

Permanent electrical resistivity tomography (ERT) monitoring systems of earthen embankments have mainly been tested by designing 2D layouts parallel to the longitudinal axis of the structure (Sjödahl *et al*., 2006; Hojat *et al*., 2019c). However, such a layout results in the distortions of 2D measured pseudosections due to 3D effects (Sjödahl *et al*., 2006; Arosio *et al*., 2018; Hojat *et al*., 2019b). This is due to the fact that 2D ERT inversion algorithms assume that the resistivity does not change in the direction perpendicular to the ERT profile (Arosio *et al*., 2018). Deviations from this assumption generate 3D effects (Sjödahl *et al*., 2006; Uhlemann *et al*., 2018). Therefore, it is necessary to quantify the site-specific 3D effects on 2D ERT profiles before inverting the data. The 3D effects are obviously present when performing 2D ERT measurements along river embankments, where, depending on the season, water and/or air is present on one side and air is present on the other side.

In this research, we estimate seasonal 3D effects for a permanent ERT monitoring system along the embankment of an irrigation canal in San Giacomo delle Segnate, Italy. Our research includes two stages. The first stage consists of numerical modelling and laboratory measurements on levee specimens designed by downscaling the real study site. Different scenarios were simulated in the laboratory, and 3D effects were calculated for each test. After validating the approach with the laboratory experiments, we moved to the second stage, which consists of calculating the seasonal 3D effects for the real site. The method we discuss in this paper is beneficial for correcting 2D ERT data for 3D effects before performing the 2D inversion. The main benefit of our approach is reducing the computational time and memory required by a full 3D inversion. This might be important in real-time monitoring, where a data set is acquired several times a day, and the inverse model is generated immediately after the data are measured. Some systems have a computerized automatic alert system which sends an alert if there is a significant change in the inverse model.

THE PILOT SITE

To permanently monitor the internal hydrogeological conditions of the embankment of an irrigation canal in San Giacomo, northern Italy, a customized ERT monitoring system was installed on 15 September 2015. The irrigation canal is very close to nearby houses and is protected by a concrete liner that covers the floor as well as the inner sides. The canal had been strongly affected by structural problems in the past requiring frequent maintenance. Therefore, the most critical part of the embankment was detected through preliminary investigations, and the designed prototype consisting of a remotely controlled low-power resistivity metre was installed. The device is a resistivity metre connected to two buried cables equipped with 48 stainless-steel plate electrodes (20 × 20 cm) spaced 1.0 m apart and buried at a depth of 0.5 m (Fig. 1a). Contact resistances were measured after installation and several other times since then, generally observing values around 0.5 kΩ, rarely approaching 2 kΩ. There is no evident increase of contact resistances in the winter, because no freezing seems to happen. The standard deviation of the measurements in the pilot site is often less than 1%. The sequence of measurements by the prototype is programmed to minimize electrode charge-up effects (Dahlin, 2000). Measurements are made level-by-level, never replacing current electrodes at measurement n with potential electrodes at measurement $n + 1$. An ultrasonic water level sensor and a weather station (red arrows in Fig. 1b) were also installed to measure temperature, rainfall and water level data in the pilot site. The system has been working since the installation day, operating remotely

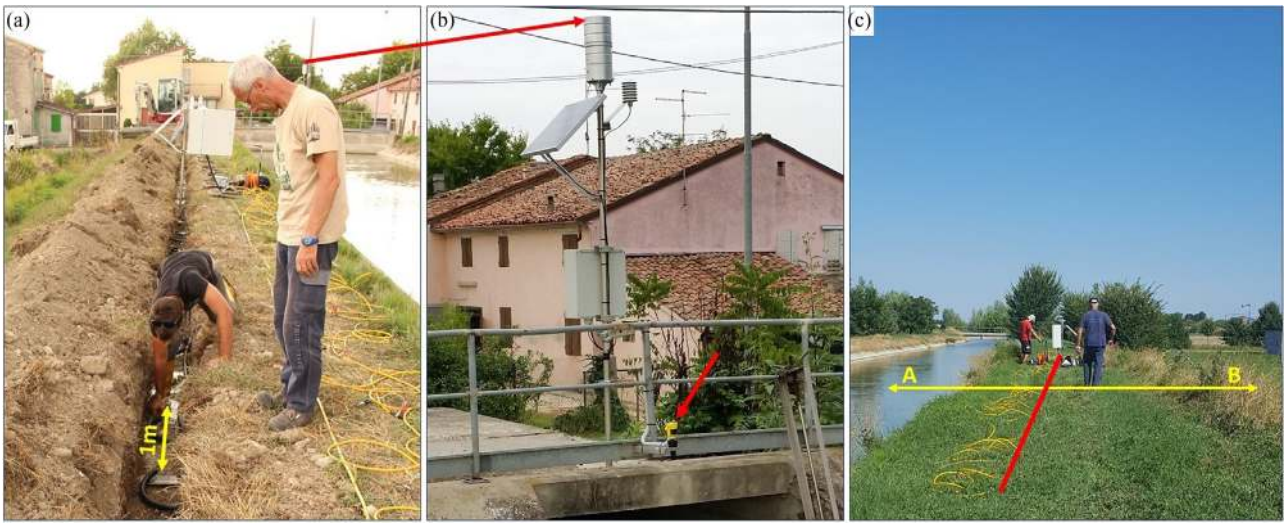

Figure 1 (a) The customized ERT system being installed along the river levee in San Giacomo. Plate electrodes are spaced 1.0 m apart and buried at the depth of 0.5 m. (b) A weather station and water level sensor (red arrows) were installed close to the ERT profile. (c) Lateral variations (yellow line) in the direction perpendicular to the ERT line (red line) that cause 3D effects: water or air or water/air on the river side (A) and mainly air on the other side (B).

and sending the measured resistivity data sets through an internet connection to provide real-time information about the saturation and seepage conditions of the monitored structure (Tresoldi *et al.*, 2019).

Figure 1(c) illustrates that, although the most practical layout is to perform ERT measurements along the river levee (red line), there are lateral variations of the media (yellow line) in the direction perpendicular to the ERT line that cause 3D effects. The material at the sides of the levee is water, air, or water and air on the river side of the embankment (A in Fig. 1c), with varying heights depending on the season, and air on the other side (B in Fig. 1c, always having a height of 3 m). The specific geometry of the study site includes a ditch near the base of the levee on side B to collect water.

LABORATORY SIMULATIONS

To explore how significantly 3D geometry may affect 2D ERT data measured along the river levee, we performed different laboratory measurements on downscaled levees. The geometry of the levee section was designed according to the real site geometry by applying a scaling factor of 1/12. The levee was constructed on a laboratory flume with transparent plexiglass walls (Scaioni *et al.*, 2018). Laboratory tests were initially performed on a levee made from homogeneous sand and later on levees made from the soil collected from the study site in San Giacomo. For resistivity measurements, we used two 24-channel mini-cables assembled in-house and terminated with 48 stainless-steel 2-cm-long mini-electrodes (Hojat *et al.*, 2019a). The cables are compatible with the commercial IRIS Syscal Pro instrument (iris-instruments.com).

Figure 2 shows an experiment in which the levee was built with uniform fine sand with an initial volumetric water content of 13%. The main aim of this experiment was to simulate different seasons. Due to the limited length of the laboratory flume, the scale was not applied to electrode spacing, and the ERT spread was laid along the levee with unit electrode spacing $a = 3$ cm. This permits using all available 48 electrode take-outs and obtaining the desired lateral and vertical data coverage with a resolution that, re-scaled to the size of the pilot site, is better than the resolution of the real spread. Since rainfall events were also simulated in this experiment, the electrodes were buried at a depth of 2 cm to prevent preferential infiltration pathways at positions of electrodes. It should be mentioned that the shape of electrodes becomes important when the ratio of electrode length/spacing exceeds 0.2 (Rücker and Günther, 2011). This threshold ratio was not satisfied in our laboratory experiments for the shallowest couple of data layers. Since the main purpose of laboratory experiments was to demonstrate the importance of 3D effects, which is not a problem of the shallowest measurements, and defining the correction strategy rather than developing the scaled numerical results, we did not consider the effect of electrode length/spacing in this paper. The

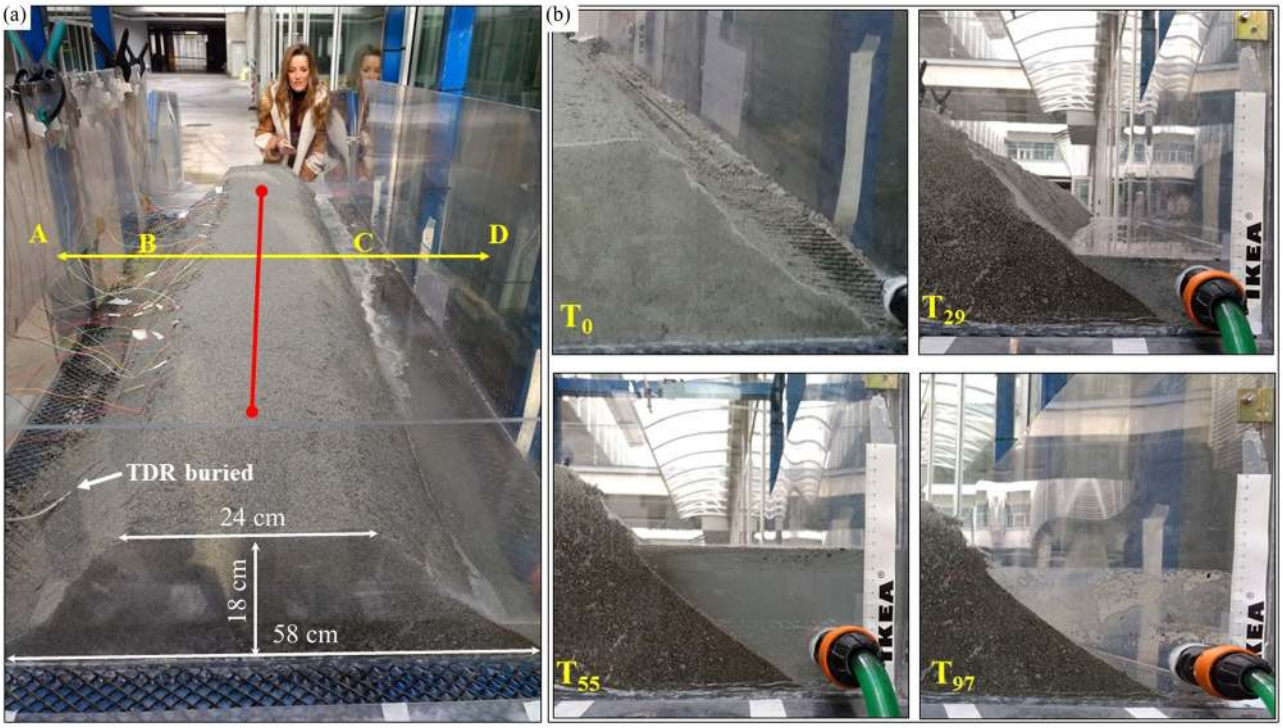

Figure 2 A laboratory experiment for a levee made from homogeneous sand. (a) ERT spread is buried at the depth of 2 cm along the levee (red line). The yellow arrow points out lateral variations in the direction perpendicular to the ERT line: A and D are the walls of the flume; B is the side of the levee filled with air; C is the river side of the levee that may be filled with air or different levels of water. The white arrow points to the approximate position of TDR buried 8 cm from the base of the levee and 8 cm far from the last electrode. (b) Different simulated conditions: T_0 = empty canal and dry levee at the beginning of the experiment; T_{29} = 5.25 cm of water in the river; T_{55} = 11.5 cm of water in the river; T_{97} = empty canal after a filling period.

acquisition sequence was programmed for measuring 10 levels using the Wenner configuration ($a = n \times 3$ cm, with n increasing from 1 to 10). A time-domain reflectometry (TDR) probe was also buried in the levee to measure time-lapse volumetric water content values (Menziani *et al.*, 1996). The white arrow in Fig. 2(a) points to the approximate position of TDR that was buried 8 cm from the base of the levee. To minimize its influence on ERT measurements, TDR was placed 8 cm away from the last electrode.

Being an irrigation canal, the monitored pilot site of this study is frequently subject to cycles of saturation and drying, experiencing seasonal variations of water level in the canal. Therefore, the measured apparent resistivity pseudosections can be affected by different 3D effects during different periods. To explore this, different situations at the river side were simulated in the laboratory. Resistivity variations within the levee were continuously monitored using the high-speed acquisition option of the IRIS Syscal Pro unit, which reduces the measurement time of a Wenner pseudosection to about 3.5 minutes. High-speed measurements are especially important in small-scale tests and considering the high permeability of the sand used in our tests. However, high-speed measurements did not provide the quality factor (the standard deviation of each measurement in percent). At the beginning, contact resistances were very high, in the order of 20–30 kΩ, because the levee was dry. However, the initial condition was also measured in standard mode, that is, by performing data stacking and by calculating the quality factor. Despite the high values of the contact resistances, the quality factor was always lower than 1.5% and the measured apparent resistivity pseudosections using the standard mode and using the high-speed mode for the dry levee were perfect replicas. At all successive times after activating rainfall events or filling the river side, we made some random checks and, as expected, contact resistances decreased very rapidly as soon as the rainfall started or water entered the canal.

To minimize electrode charge-up effects (Dahlin, 2000), a measurement sequence was defined so that the first electrode was kept fixed as the current electrode A, and all possible measurements with this first electrode were made moving

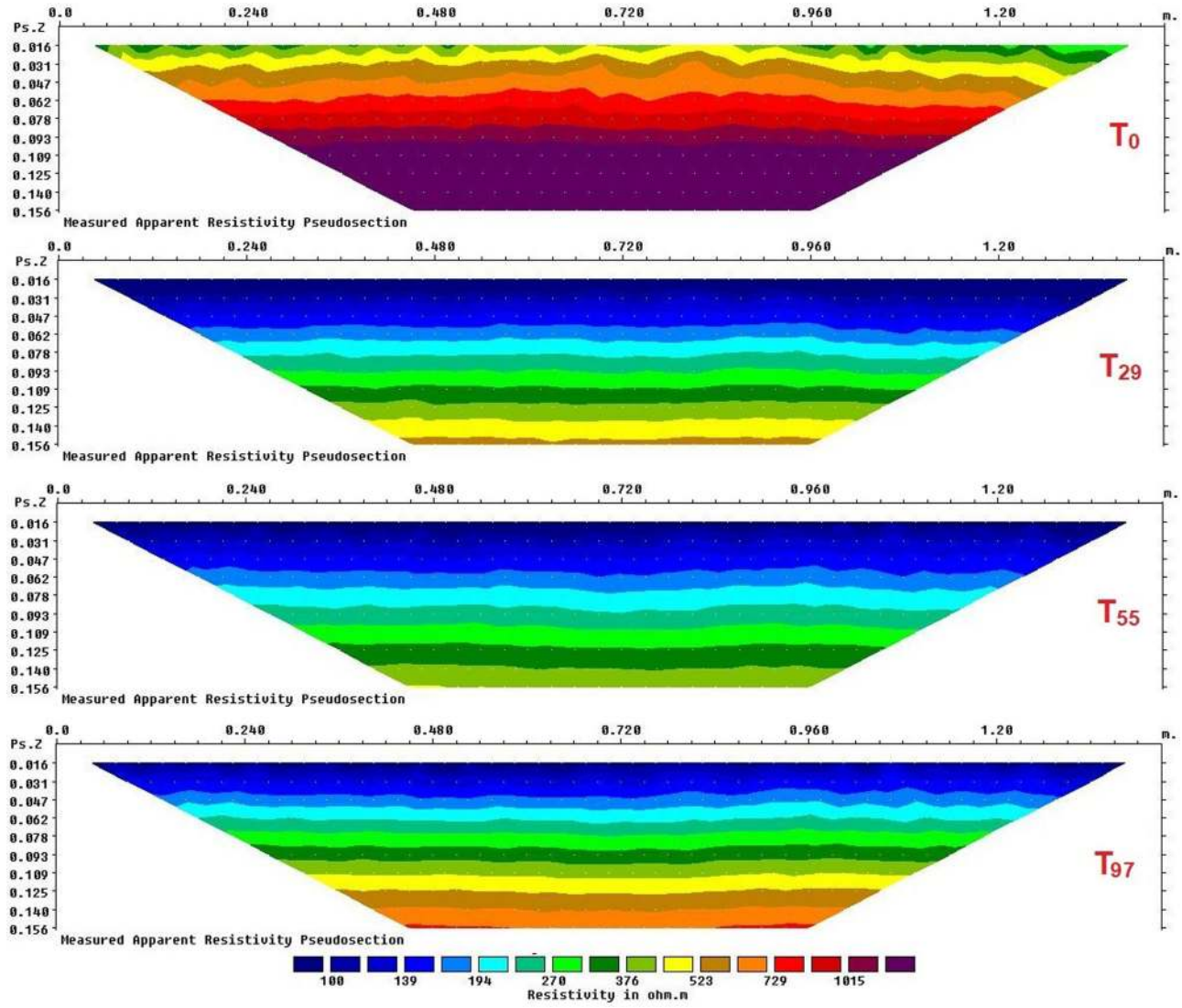

Figure 3 Measured apparent resistivity pseudosections at T_0, T_{29}, T_{55} and T_{97} for the tests shown in Fig. 2. All pseudosections are plotted with the same colour scale to facilitate comparison.

from the largest electrode spacing to the smallest spacing. Then, the measurement sequence was moved one electrode spacing to the right, making measurements with the same order. Therefore, measurements were performed diagonally, moving from the deepest point to the shallowest point for each line. Different conditions simulated in this experiment for filling/emptying periods are illustrated in Fig. 2(b): T_0 corresponds to the beginning of the test when the canal was empty and the levee material was almost dry; T_{29} shows the situation after 29 minutes from the beginning of the test when the water height was 5.5 cm in the canal; T_{55} is the time when the water height was 11.5 cm in the canal; and finally, T_{97} shows the situation 1 hour and 37 minutes from the beginning of the test when the canal was empty again, but immediately after a filling period. Thus, a careful look at Fig. 2(b), to compare T_0 and T_{97}, shows that the canal is empty at both times but the levee material is quite wet at T_{97} because it has experienced a recent filling period.

The measured apparent resistivity pseudosections at T_0, T_{29}, T_{55} and T_{97} are illustrated in Fig. 3. At T_0, when the canal is empty and levee body has an initial volumetric water content of 13%, we expect a uniform distribution of resistivity in the levee (around 350—400 Ωm). At T_{29}, the canal is filled with water up to the height of 5.5 cm. Therefore,

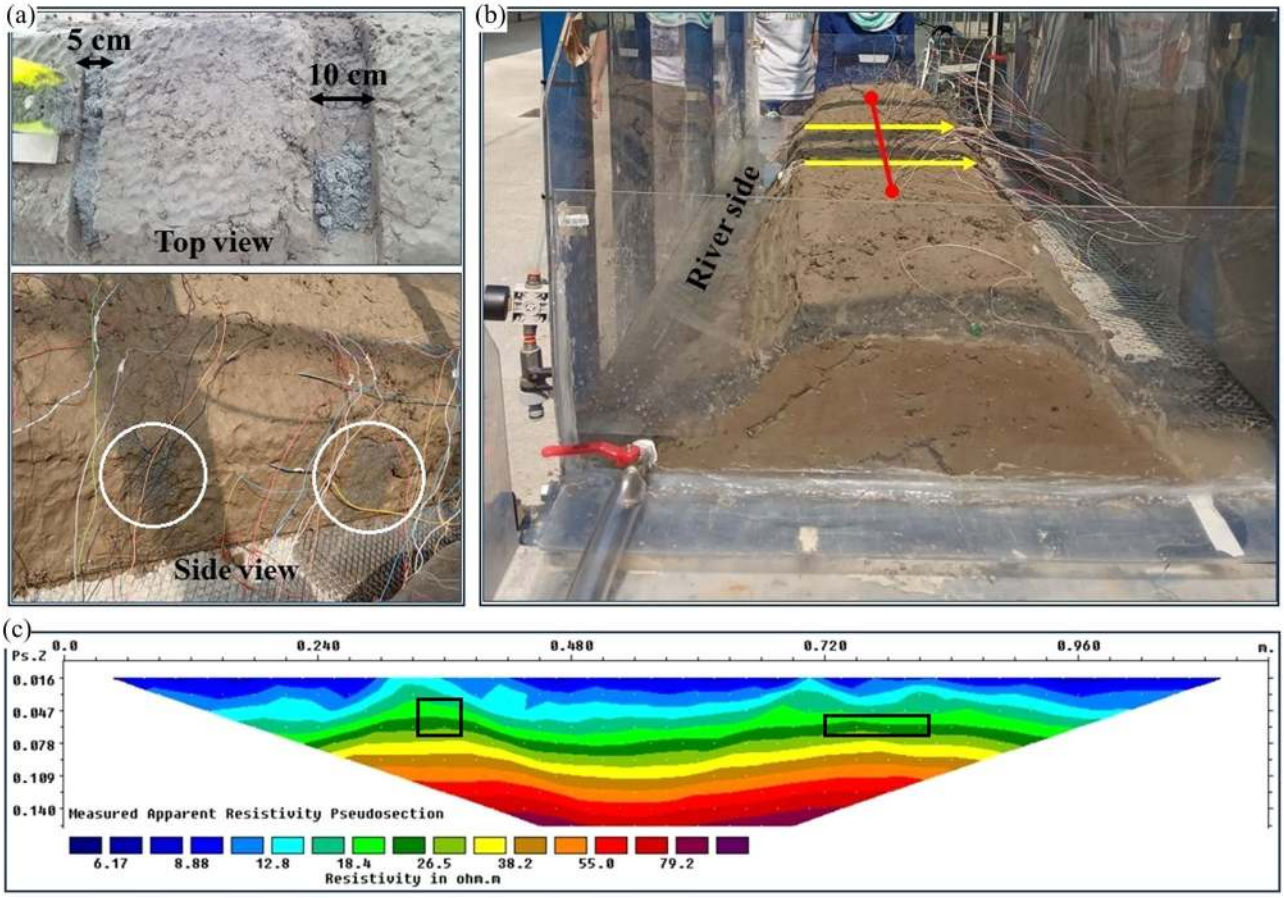

Figure 4 An example of experiments with levees made from the clayey soil of the study site. (a) Two seepage zones filled with sand were created during construction. (b) ERT spread is placed on the surface (red line) and the yellow arrows show the location and direction of the seepage zones. (c) Measured apparent resistivity pseudosection before adding water to the river side, T_0 (black rectangles show seepage zones).

the permeable sand drains water, which causes the resistivity of the levee to be decreased. The height of water in the canal is increased to 11.5 cm at T_{55}. The levee is considerably saturated at this time, and we expect low resistivity values. Finally, at T_{97}, the canal is empty again, but the levee body is expected to be saturated, and thus it should be much more conductive compared to T_0. The measured apparent resistivity pseudosections shown in Fig. 3 are reflecting the general expected reduction in resistivity values after T_0, but the details are masked in all these pseudosections by an anomalous increase in resistivity values with depth. Such unusual vertical gradients in measured values significantly disturb the real resistivity distribution in the levee and are due to 3D effects as well as the effect of the resistive base of the laboratory flume which is actually an insulating boundary.

In 2D ERT surveys, it is assumed that the resistivity does not change in the direction perpendicular to the ERT line. However, as shown in Figs 1(c) and 2, considerable changes are also present in the direction perpendicular to the strike of the embankment. For the laboratory tests, another specific issue is the influence of high-resistivity side walls of the flume, which is again a 3D effect in nature (Arosio *et al.*, 2018). In these situations, 2D ERT models cannot distinguish between the actual changes of the resistivity with the depth and those produced by 3D effects. Therefore, it is necessary to quantify seasonal 3D effects for any site-specific geometry. The 2D ERT data sets must then be corrected for 3D effects before being inverted (Hojat *et al.*, 2019b). Besides, for the specific set-up of the laboratory tests in our study, the base of the flume is covered by plexiglass, which is an electrically resistive material. This also contributes to the increasing trend of resistivity values with depth (Hojat *et al.*, 2019a).

Figure 4 shows an experiment in which the levee was built with the clayey soil collected from the study site. Two seepage

zones, 5 cm and 10 cm wide, crossing the levee were created during the construction of the levee. The seepage zones were filled with sand and covered with a top layer of clay so that they were embedded in the levee structure (Fig. 4a, top). Considering the significant contrast in permeability of sand with the hosting clayey material, the two sandy zones could be considered as anomalous seepage zones. The side view at the exit of seepage zones shown in Fig. 4(a) shows the moment when water is exiting from the wider seepage zone and arriving at the smaller seepage zones (white circles). Similar to all our laboratory experiments, Wenner array with minimum electrode spacing $a = 3$ cm was used for ERT measurements. The ERT spread was located at the surface (Fig. 4b), because no rainfall was simulated in this test. Due to a problem of cable failure, we had to use only 39 electrodes for this test. The level of water in the river side was increased to the maximum height, and it was kept constant until the water was continuously flowing out from both seepage zones. This experiment also tested the capability of fibre optics in sensing water leakage (Hojat *et al.*, 2019d). Time-lapse ERT data were measured every 3 min using the high-speed option of the Syscal Pro instrument. Again, high-speed measurements did not provide the quality factor, but we performed a couple of check measurements at random times. Contact resistances at the beginning of this test were around 1–2 kΩ. The measured apparent resistivity pseudosection before adding water in the river side (T_0) is illustrated in Fig. 4(c). We expect a uniform distribution of low resistivity for the levee body at T_0 with two anomalous dry sand zones. Similar to the previous example, the details of measured apparent resistivity pseudosection shown in Fig. 4(c) are mainly masked by an anomalous increase in resistivity values with depth. Therefore, we see again how 3D effects and the effect of the insulating base of the laboratory flume disturb the measured data. These effects were observed in all measured apparent resistivity pseudosections.

QUANTIFYING 3D EFFECTS

To quantify 3D effects for the experiment shown in Fig. 2, a 3D levee and its boundary conditions at each measurement time (different levels of water on the river side and mainly air on the other side) were reconstructed in RES3DMODx64 (Loke, 2014). One specific feature for our laboratory tests is that the side walls of the laboratory flume are made from resistive plexiglass. Therefore, side walls were also included in the 3D models, defined as borders with high-resistivity values similar to the air. Since homogeneous sand was used to construct the levee for this experiment and the sand almost uniformly got wet when there was water in the canal, the synthetic models for each time were defined for a homogeneous structure. The resistivity value selected for each model was the average value of measured apparent resistivity values at shallow depths for the corresponding measurement time. To also consider the effect of the insulating base of the laboratory flume in the synthetic 3D models defined in RES3DMODx64, the bottom of the levee was confined to a plane with the high-resistivity value used for air (250,000 Ωm) extended in the vertical direction. The difference between defining an insulating boundary and replacing the boundary with a high-resistivity layer was checked by testing the two solutions with RES3DMOD. We found that using 250,000 Ωm for side walls and the base generates differences between the two models that in the worst case are about 0.2%. This occurs for the measurements with the largest electrode spacing and when the levee is more resistive, that is, when we simulate the initial dry condition. Since 0.2% is lower than the expected noise affecting real measurements, we concluded that replacing the insulating boundaries (bottom and lateral sides of the flume) with very high resistive material was a valid approach.

After defining the models, the apparent resistivity pseudosections were calculated for the profile in the middle of the levee along its crest at each measurement time. Figure 5(a) illustrates the graphs of the ratio of apparent resistivity values calculated in RES3DMODx64 at each time divided by the homogeneous resistivity value defined for the levee material at similar time. If we divide the apparent resistivity values measured at the laboratory by the values of Fig. 5(a) for the corresponding time, we will remove the 3D effects and the effect of the insulating bottom of the flume from the measured data sets. Considering that in the real site, we mainly have 3D effects rather than a resistive bottom layer or an insulating base, we followed a similar procedure to quantify only 3D effects. For this purpose, we defined 2D synthetic models in RES2DMOD (Loke, 2016), adding the vertically extended plane with the high-resistivity value of the air below the homogeneous levee for each measurement time. Figure 5(b) illustrates the graphs of the ratio of apparent resistivity values calculated in RES3DMODx64 for each time divided by the apparent resistivity values calculated in RES2DMOD at the same time. Since both 3D and 2D synthetic models used to obtain the graphs shown in Fig. 5(b) include the insulating base of the laboratory flume, these graphs only reflect the 3D effects due to the levee geometry and its lateral boundary conditions. The levee body was almost homogeneous at each depth level and thus the graphs shown in Fig. 5 are plotted

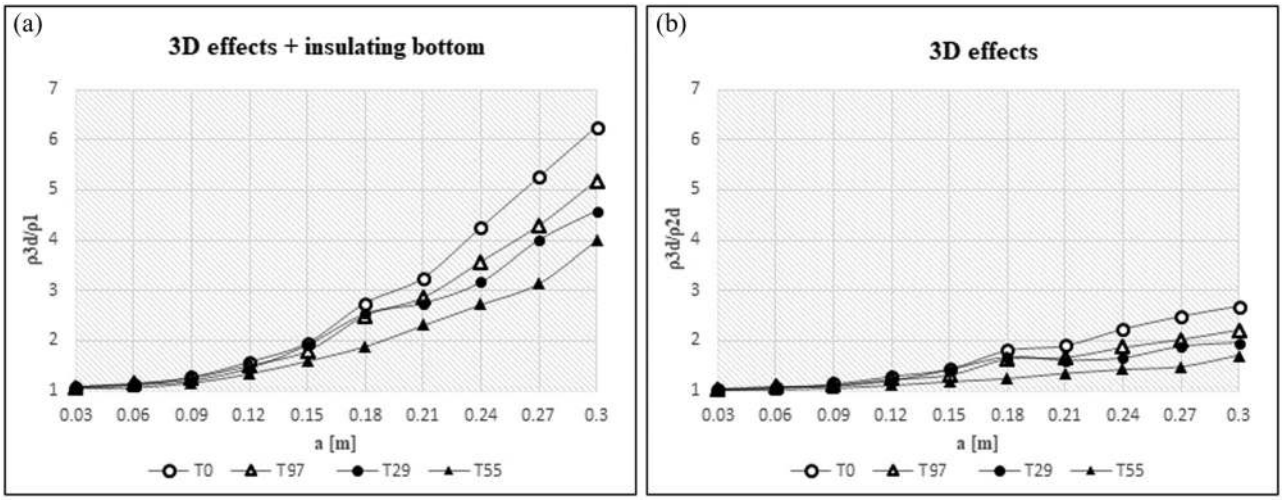

Figure 5 Graphs of the ratios of apparent resistivity values for different measurement times of the experiment shown in Fig. 2: (a) Apparent resistivity values calculated in RES3DMODx64 divided by the measured apparent resistivity of the top layer. (b) Apparent resistivity values calculated in RES3DMODx64 divided by apparent resistivity values calculated in RES2DMOD for a model simulating the levee over an insulating base.

for resistivity ratios versus electrode spacing (associated with the penetration depth).

Figure 5(a) shows that in the special case of laboratory tests in a flume with insulating borders, measured apparent resistivity values can be amplified by a maximum factor of 4.00–6.25 depending on the season. By considering the 3D effects only (Fig. 5b), we observe that resistivity measurements are still significantly disturbed being amplified by a maximum factor of 1.5–2.7 depending on the season. The presence of an insulator below the levee is not the situation that we actually encounter in real sites and, therefore, Fig. 5(b) is closer to the conditions of the study site. Note that the estimated 3D effects for laboratory tests not only reflect the effects of lateral air and/or water on the sides of the levee, but also include the effect of the insulating side walls of the laboratory flume. It can be understood from Fig. 5(b) that 3D effects increase as the electrode spacing is increased. This is obviously because the effect of the material perpendicular to the ERT line increases with electrode spacing. As a result, the deeper parts of the 2D models are more distorted due to the off-axis changes. Note also the variability of 3D effects at different times corresponding to different levels of water in the canal during different seasons. The amplification factor decreases in scenarios where water is present in the canal (T_{29} and T_{55}) due to the fact that the contrast between resistivity of the soil and water resistivity is lower than that between the soil and air. The largest 3D effects are observed at T_0 when the canal is empty and the levee material is almost dry, while the lowest 3D effects are observed during the time of highest water level in the canal (T_{55}).

The 3D effects were quantified for all laboratory experiments using the general concept discussed above. To quantify 3D effects for the experiment shown in Fig. 4, 3D geometries for each measurement time were reconstructed in RES3DMODx64 (Loke, 2014) and the apparent resistivity pseudosections were calculated for the profile in the middle of the levee along its crest. In this experiment, the levee body is not homogeneous at each depth level due to the presence of seepage zones. Therefore, synthetic models took into account a clay material hosting two sand zones. At each measurement time, the 3D model defines the clayey levee, two seepage zones, the insulating side walls and bottom of the flume, and the level of water in the canal at that time. Similarly, 2D models were not defined for a homogenous levee and they considered the seepage zones. Two different groups of 2D models were defined in RES2DMOD: (i) the levee body over a vertically extended high-resistivity plane to explore only 3D effects, and (ii) the levee body without any layer below to calculate the combined influence of 3D effects and of the insulating bottom of the laboratory flume. Apparent resistivity pseudosections were calculated for all 2D models. As an example, Fig. 6(a) shows measured apparent resistivity pseudosection for T_0 of the test shown in Fig. 4 and the calculated apparent resistivity pseudosection for this time obtained from simulations in RES3DMODx64. Considering the laterally heterogeneous structure of the levee in this test, amplification ratios of the

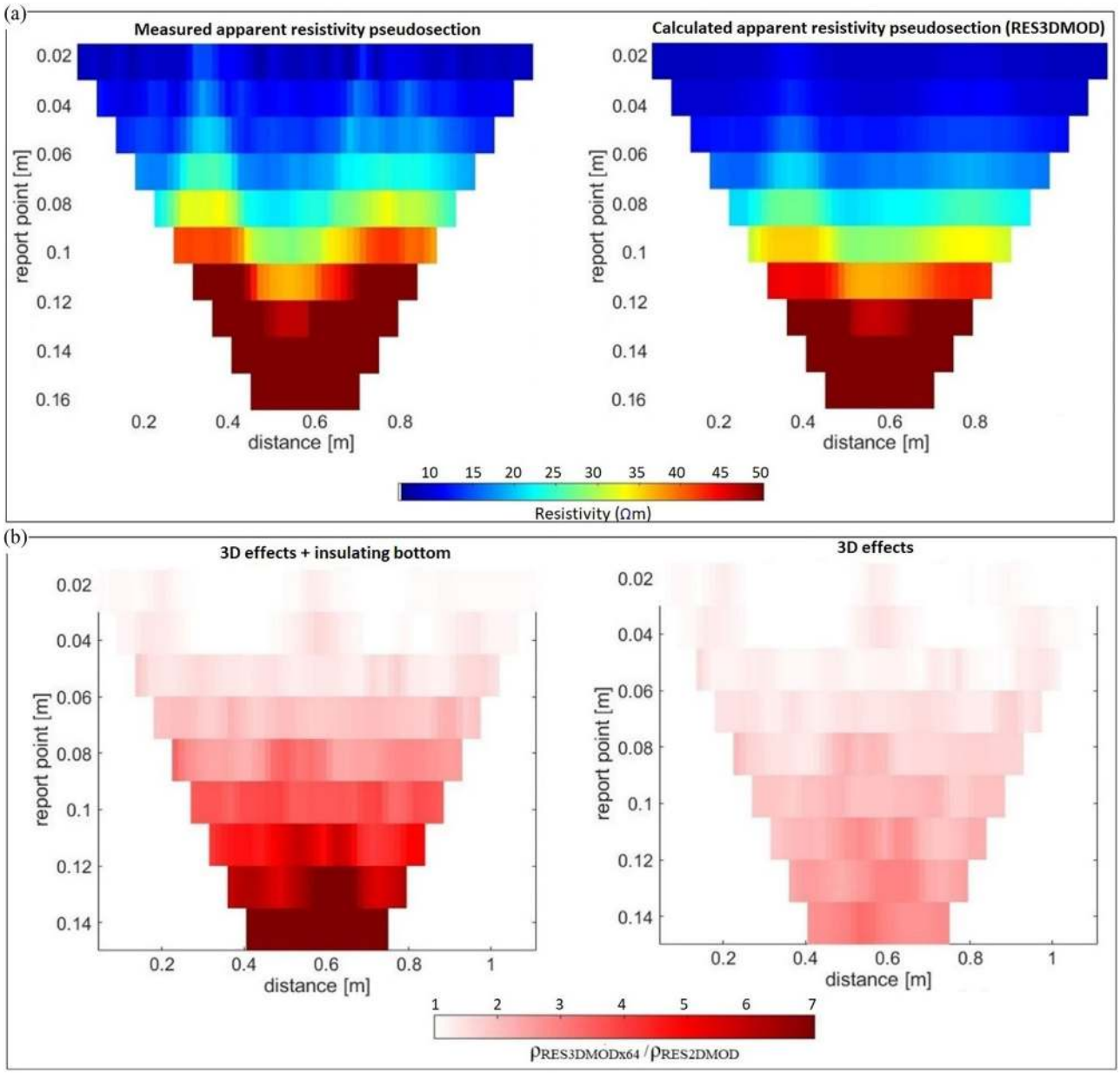

Figure 6 (a) Measured apparent resistivity pseudosection and apparent resistivity pseudosection calculated in RES3DMODx64 at T_0 for the experiment shown in Fig. 4. (b) Pseudosections of the ratio of apparent resistivity values calculated in RES3DMODx64 divided by the apparent resistivity pseudosection calculated in RES2DMOD for a levee with infinite depth (left) and for a levee over an insulating base (right).

measured apparent resistivity values were calculated for each point rather than being averaged for each electrode spacing, as was the case shown in Fig. 5. The calculated apparent resistivity pseudosections obtained from RES3DMODx64 were divided by the calculated apparent resistivity pseudosections obtained from RES2DMOD for both synthetic 2D models (with and without the insulating base). Figure 6(b) illustrates the pseudosections of the ratios of apparent resistivity values at T_0 reflecting amplification of the measured apparent resistivity values due to 3D effects plus the influence of the insulator at the bottom of the laboratory flume (left), and due to 3D effects alone (right). Note again that the effect of the side walls of the laboratory flume is also included in 3D effects.

Having assessed the importance of 3D effects and their variations with seasonal conditions at the laboratory scale, we

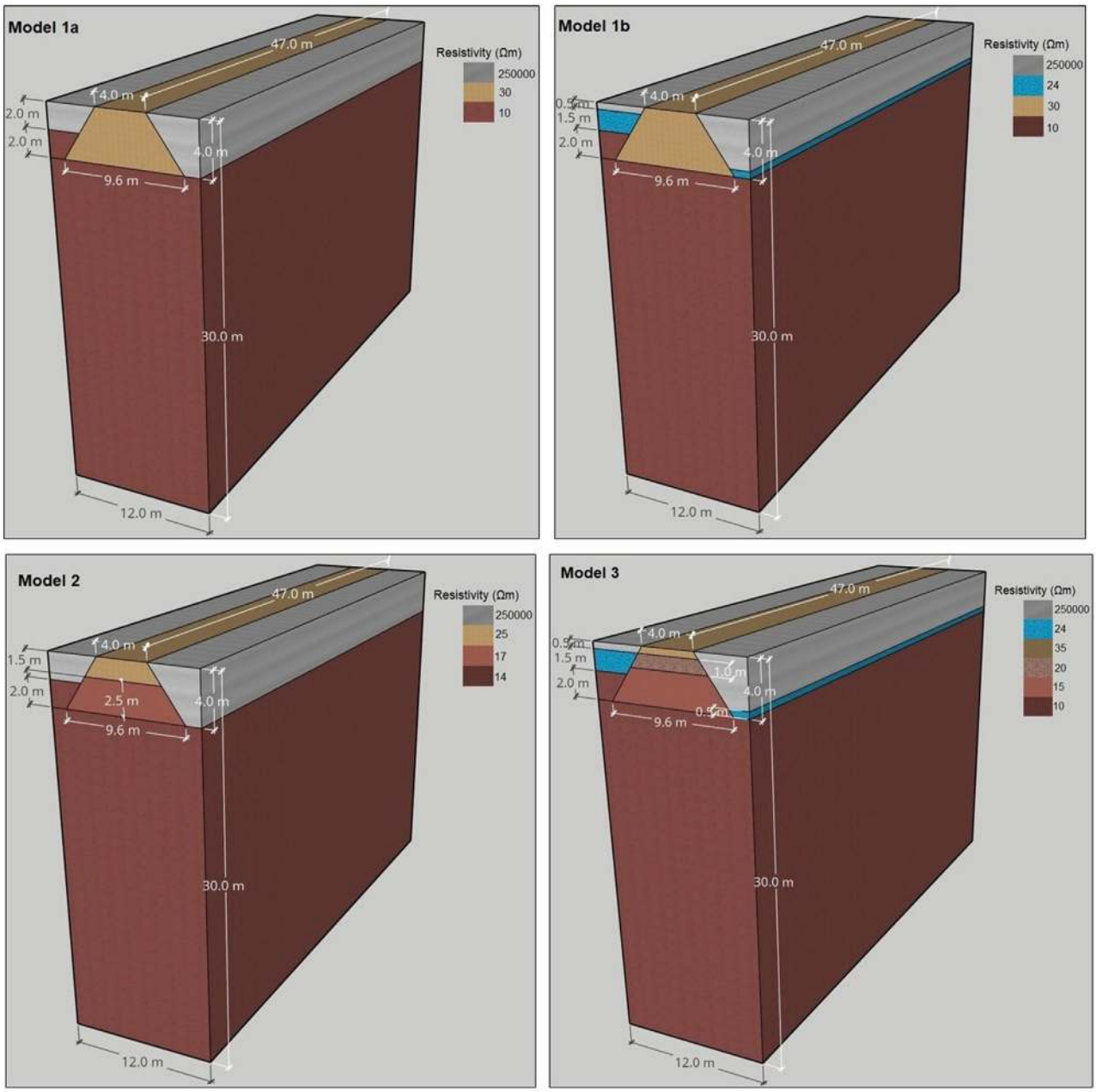

Figure 7 3D geometries used to calculate seasonal 3D effects for the pilot site. Grey and blue parts demonstrate air and water, respectively.

applied the same procedure to quantify seasonal 3D effects for the real site. Drones were used to accurately reconstruct the morphology of the monitored levee. The flights were carried out at the height of 30 m, guaranteeing a ground resolution of a few centimetres. The DEM file was associated with the ortophoto data and provided information about the distances and elevations. Ground control points measured with Global Navigation Satellite System–Real-Time Kinematic (GNSS–RTK) were used for calibration and quality check of drone measurements. The resulting accuracy of the DEM file is in the order of a few centimetres. After obtaining the accurate geometry of the study site, 3D effects were calculated by testing different models for the levee body. All models extend well below the levee body through a clay soil. Synthetic 2D and 3D models of the pilot site were constructed in RES2DMOD and RES3DMODx64, respectively, for different seasons. A

47 × 12 × 30 m 3D model (Fig. 7) was defined including 48 electrodes along the ERT profile (x direction) with the minimum electrode spacing $a = 1.0$ m, and 16 grid points in the direction perpendicular to the ERT profile (y direction) with the spacing of 0.8 m. The model depth was extended down to 30 m. The 2D model was defined with the same grid size along the x direction and depth. The design of the levee structure in the synthetic models was based on core samples extracted from the levee as well as considering expected changes in saturation of the levee during different seasons. Four different models were defined (Fig. 7): a homogeneous levee located on a conductive layer with empty canal during winter (model 1a) and filled canal during the irrigation period (model 1b); a two-layered model for the levee during winter (model 2); and a three-layered model for the levee during the irrigation period (model 3). The homogeneous levee assumed in models 1a and 1b helps understanding the 3D geometry effects prior to introducing the influence of a more complex structure for simulating the levee body. Models 2 and 3 represent more realistic situations that take into account the granulometric variations with depth observed on a few core samples and the changes in levee body saturation throughout the year. Different from model 2, an additional thin upper layer was introduced in model 3 to simulate the upper part of the levee which is quite dry (and thus more resistive) during the summer. The middle part of the levee is saturated during summer, when the canal is filled with water for the irrigation period, and relatively dry during winter due to the absence of water in the canal. The base of the levee is mainly composed of clayey and silty materials and during the whole year shows low resistivity values. The resistivity values set for each model are shown in Fig. 7 on the right side of each model. The selected resistivity values were defined through a trial-and-error procedure aimed at obtaining a good match between apparent resistivity values calculated from forward modelling and the values measured in the site. Resistivity of the water flowing in the canal was measured in laboratory resulting in 24 Ωm. Air was modelled as a very high resistive material (250,000 Ωm). The maximum difference in the apparent resistivity values calculated by directly adding the topography in the 3D forward model and using the high resistivities to model the air is only about 0.2%. It is easier to construct the model by using high values for the cells used to model the air and a flat top model as Res3dmodx64 does not have an option to visualize the topography. If the topography option is used, the depths to a layer will change following the topography, so it needs more work to make sure that flat layers like the water layer remain flat in 3D.

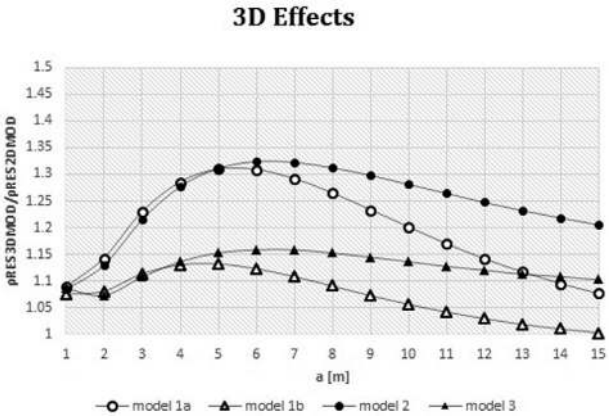

Figure 8 Graphs of the ratio of apparent resistivity values calculated with RES3DMODx64 to those calculated with RES2DMOD for the different models shown in Fig. 7.

Apparent resistivity pseudosections were calculated for each 2D model in RES2DMOD and also along the central profile for each 3D model in RES3DMODx64. Figure 8 illustrates the graphs of the ratio of apparent resistivity values calculated in RES3DMODx64 to those obtained from RES2DMOD plotted versus the electrode spacing. It is observed that for all the four defined models, as the electrode spacing is increased, 3D effects increase up to a maximum value, and then begin to decrease for the deepest measurements. This is because, as the electrode spacing is increased from smallest values up to the spacing corresponding to penetration depth equal to the height of the levee, 3D effects increase due to the lateral inhomogeneities present on two sides of the levee. On the contrary, a further increase in electrode spacing, and the associated increase in penetration depth, results in a decrease in the percentage of the volume occupied by lateral inhomogeneities on two sides of the levee height (air and water) compared with the volume of the soil affected by current flow. Thus, 3D effects start to decrease. Similar to the general concept as understood from the laboratory experiments, a comparison of curves in Fig. 8 shows that 3D effects are larger during winter when the irrigation canal is empty, reaching a maximum of about 30%, and lower during summer when water is flowing in the canal, reaching a maximum of about 15%. This is because the resistivity of the levee material (ranging within 15–35 Ωm) is very close to the resistivity of the water in the canal (24 Ωm). Therefore, during the irrigation period, when the canal is filled with water, 3D effects are mainly coming from the side where there is air with a considerably higher resistivity contrast. In the winter, on the other hand, air is present on both sides of the levee,

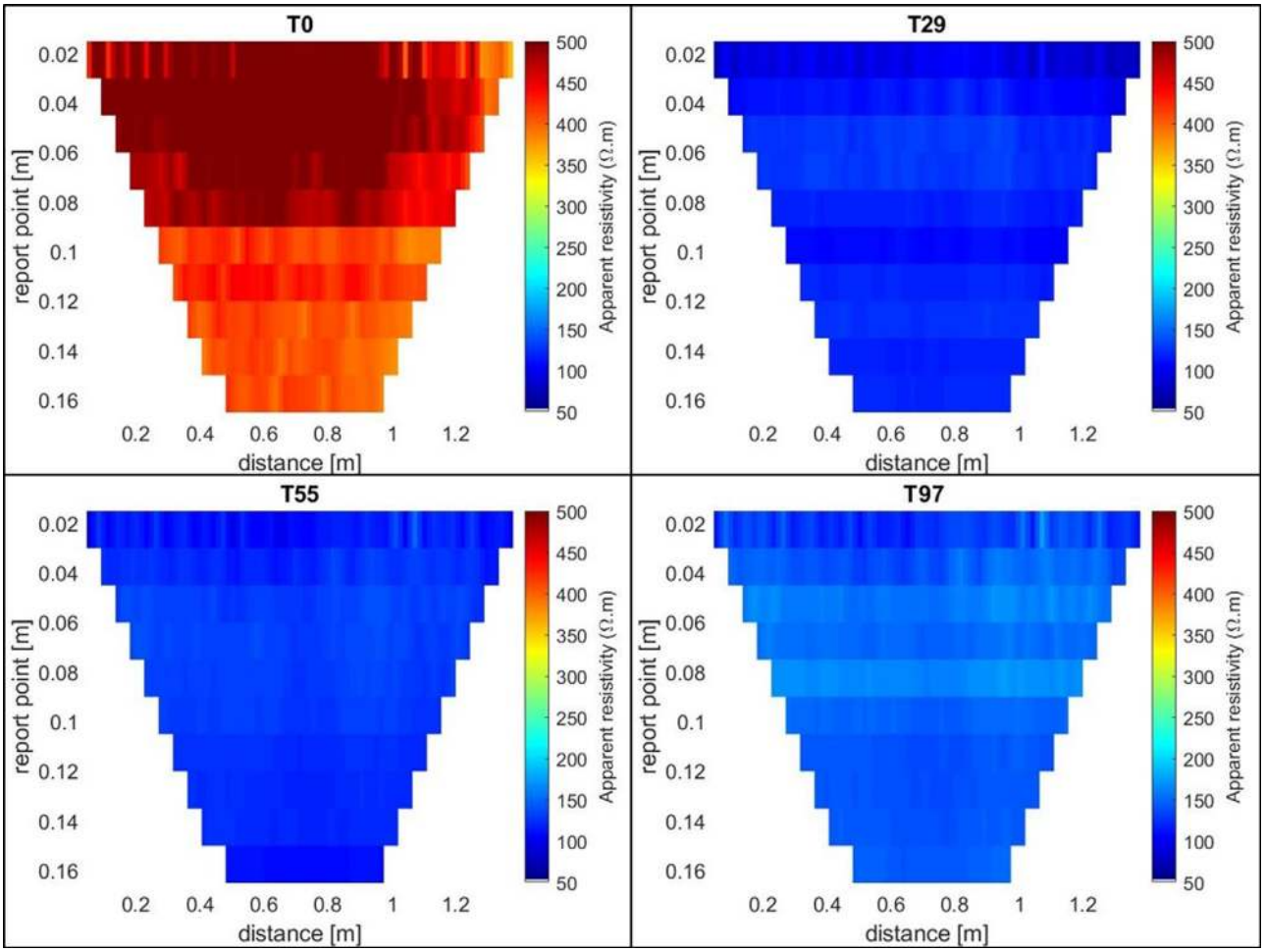

Figure 9 Measured apparent resistivity pseudosections of the experiment shown in Fig. 2 corrected for buried electrodes and 3D effects.

and this higher contrast in resistivity values gives rise to 3D effects.

Finally, comparing the graphs for homogeneous models with graphs calculated for layered models shows that 3D effects vary not only due to lateral changes but also due to the composition of the levee material (i.e. on the resistivity distribution in the levee body).

3D CORRECTIONS AND INVERSION

Figure 5(a) was used to correct apparent resistivity pseudosections measured in the laboratory for the experiment shown in Fig. 2. As mentioned in the laboratory set-up, the electrodes were buried for this experiment. It is known that when using buried electrodes, the effect of the overlaying layer should be taken into account. When electrodes are located on the surface, the current flows only in the lower half space, but when the electrodes are buried, the current also flows in the soil layer above the electrodes. The effect of soil above electrodes can be quantified by the analogy between the electrical situation and optics (Telford *et al.*, 1990). We used this concept, and assuming a Wenner array with unit electrode spacing $a =$ 3 cm and electrodes buried at 2 cm depth, we calculated the ratio of apparent resistivity measured by buried electrodes, using the standard geometrical factor ($2\pi a$), to resistivity of the half space. This ratio is equal to the ratio between the geometrical factor for surface electrodes and the geometrical factor that should be used for buried electrodes. Thus, this ratio was used to correct measured apparent resistivity values for the effect of buried electrodes (Arosio *et al.*, 2018; Hojat *et al.*, 2019a). Then, for each data set, the values at each electrode spacing were divided by the ratio calculated on the related graph of Fig. 5(a) for the measurement time. Figure 9 illustrates corrected pseudosections for raw data shown in

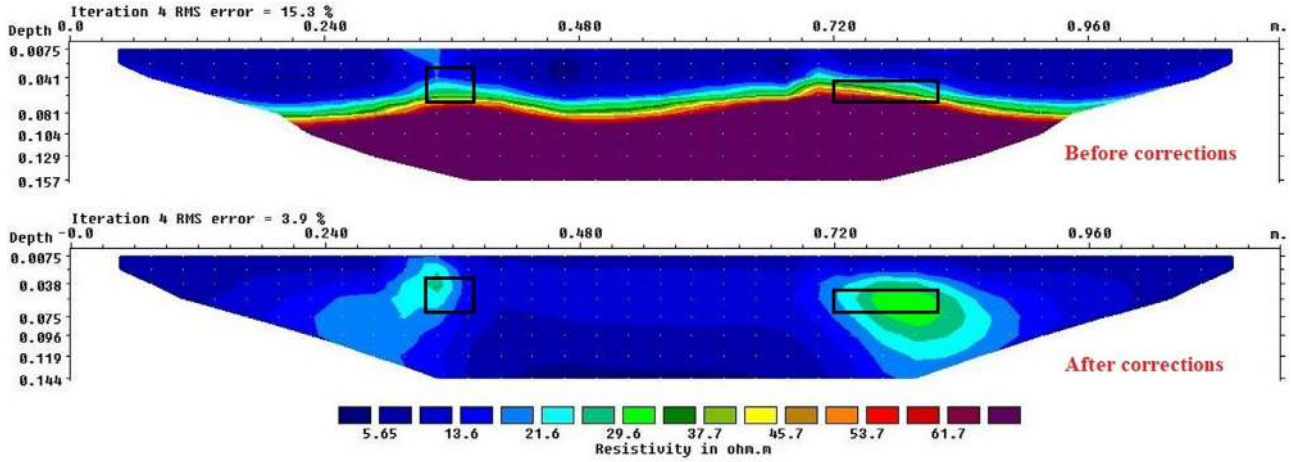

Figure 10 Inversion of measured apparent resistivity values at T_0 for the test shown in Fig. 4, before (top) and after (bottom) correcting for the effects of 3D geometry and the insulating base. Black rectangles show seepage zones.

Fig. 3. It is seen that the corrected apparent resistivity pseudosections now reflect reasonable changes in resistivity values. The corrected pseudosection at T_0 basically shows the most resistive situation for the levee body for almost dry sand. Minor inhomogeneities are due to nonuniform compaction of the soil when constructing the levee. Pseudosections measured at T_{29} and T_{55} can now clearly demonstrate reduction of resistivity values due to the saturation of the levee body because of water in the river side. Their similarity demonstrates the high permeability of the levee material that rapidly drains water from the half-filled canal up to the top of the levee body at T_{29} so that levee saturation cannot change significantly at T_{55} when the water level in the canal is higher. Resistivity values slightly increase at T_{97} immediately after the canal is empty and the water has started to drain out of the levee body. The results show that aside from some minor changes due to nonuniform compaction, resistivity values are more or less similar for each level and no significant distortion is observed due to TDR buried inside the levee in this experiment.

Figure 6(b) was used to correct the effects of 3D geometry and the insulating bottom on the measured apparent resistivity pseudosections for the experiment shown in Fig. 4. At each measurement time and for each data point, the measured apparent resistivity pseudosection was divided by the pseudosection of the resistivity ratio (left image in Fig. 6b). Figure 10 shows the results of inverting measured apparent resistivity values using RES2DINV software (Loke, 2018) for T_0 before and after 3D corrections. The importance of applying 3D corrections is well recognized in Fig. 10. Inversion of data without correcting for 3D effects results in a section which is anomalously resistive from the depth of about 6 cm. This is not a reflection of the real resistivity distribution in the levee body, and it is caused by the combination of 3D effects and the insulating base. When the data are corrected for these effects and inverted again, a meaningful resistivity distribution is obtained. Resistivity values now fall within a reasonable interval range for a clayey levee and the two sand channels embedded in the levee are clearly detected as more resistive anomalies.

Apparent resistivity values measured along the pilot site in San Giacomo were first corrected for the effect of buried electrodes following the method described by Arosio *et al.* (2018). Then, similar to the correction concept used for laboratory tests, Fig. 8 was used to correct 3D effects for these data sets. Depending on the time of each measurement (summer or winter), the apparent resistivity values at each electrode spacing were divided by the ratio calculated for the related measurement period. The graphs obtained for layered models were preferred to apply the corrections because the apparent resistivity pseudosections calculated in RES3DMODx64 for layered models were very similar to the apparent resistivity pseudosections measured at the site, meaning that the real situations were reasonably modelled by synthetic models. Figure 11 illustrates examples of apparent resistivity pseudosections measured on 29 February 2016 and 12 July 2016 before and after applying 3D corrections. The importance of applying 3D corrections can be appreciated by observing that the apparent resistivity values for the clay soil below the levee, basically unaffected by the presence or absence of water in the canal, become very similar on two images after the corrections, while before corrections the apparent resistivity images

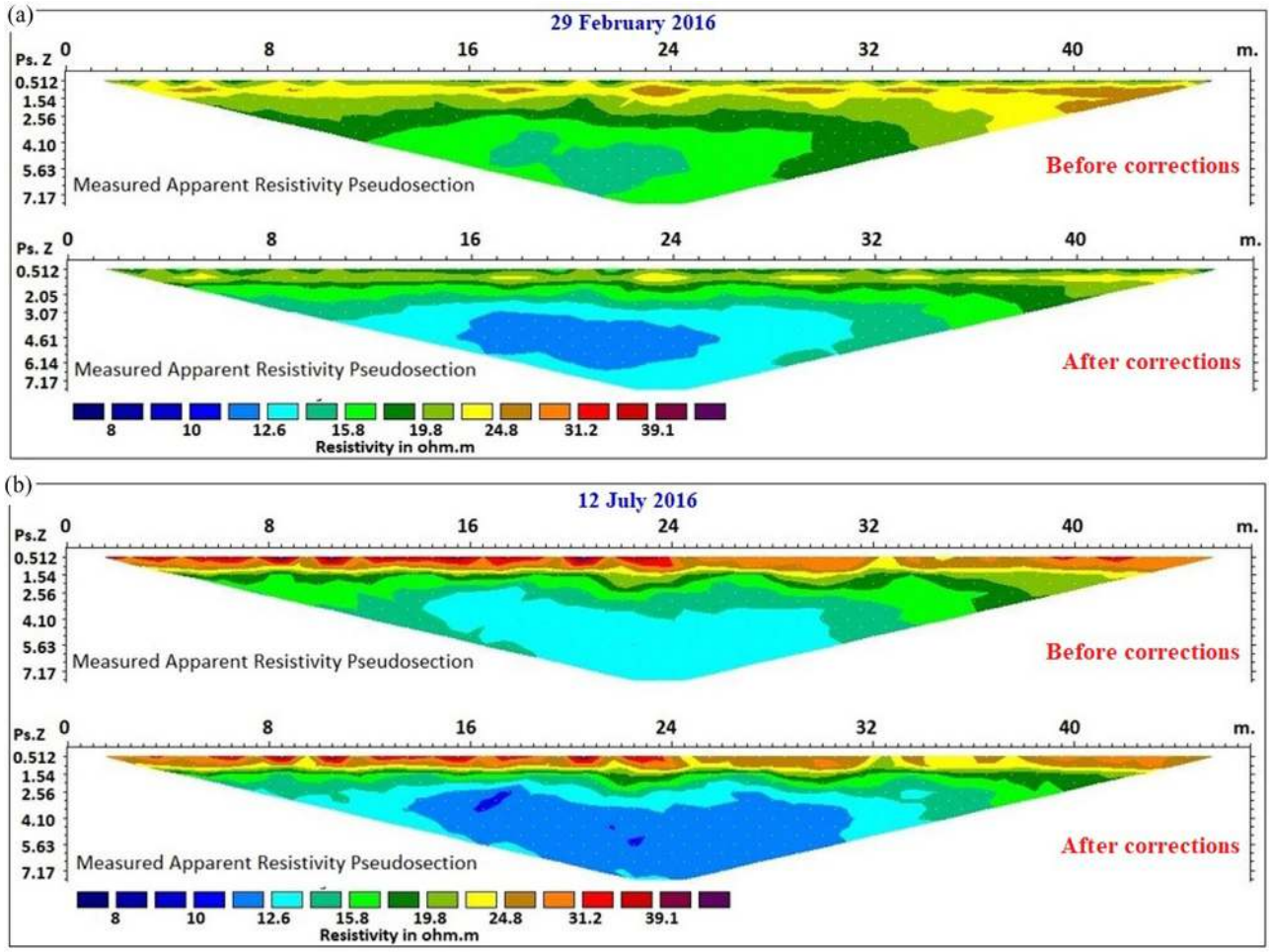

Figure 11 Examples of apparent resistivity pseudosections before and after applying 3D corrections for data sets measured along the pilot site on (a) 29 February 2016 and (b) 12 July 2016. The data were already corrected for buried electrodes.

were showing a difference which was mainly due to higher 3D effects in winter than in summer.

Graphs of Fig. 8 are being used to correct all measured apparent resistivity pseudosections obtained along the pilot embankment. Corrected data sets can be then inverted to obtain realistic resistivity images and more reliable results. This is especially important when we want to quantify water saturation in the levee by converting resistivity images into water saturation images (Tresoldi *et al.*, 2019). Before inverting the data, data sets are cleaned for negative resistance values, bad quality factors (standard deviation larger than 2%) and extremely low current. To filter out data outliers, histograms of RMS error statistics available in RES2DINV (Loke, 2018) are used after inversion.

The resistivity to water content conversion is obtained by applying a site-dependent function calibrated by Tresoldi *et al.* (2019). The calibrated function was developed using the core samples taken from the study site down to the bottom of levee, and it is therefore applicable only down to 3 m. Figure 12 illustrates the water content maps calculated for the data shown in Fig. 11. Comparing the two water content maps for 29 February 2016 and 12 July 2016, it is seen that soil water content of the shallowest layer is higher in winter (26% compared to about 15%–20%). This is due to increased precipitation and lower evaporation in this period. The distribution of soil water content at medium depths (between 1.5 and 2.5 m) is more homogeneous during winter (around 20%–22%), while in the summer, which is the irrigation season, the situation is less uniform, with zones of preferential seepage and water accumulation, especially occurring at 2.0–2.5 m, where water content arrives at about 28% versus 22% during winter. The deepest layer of the levee shows the highest

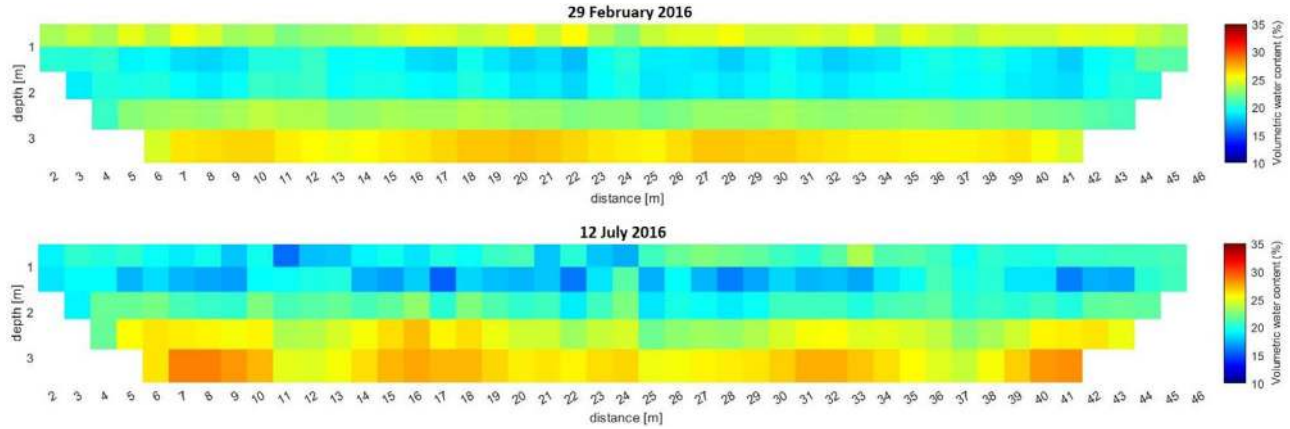

Figure 12 Volumetric water content maps calculated from corrected data shown in Fig. 11. The sections are displayed down to 3 m depth, corresponding to the levee height.

water content in both seasons. This is due to rainfall water infiltration to the base of the levee from the canal and the guard ditch in winter and due to water flowing in the canal in summer.

CONCLUSIONS

This study showed that 3D effects significantly disturb 2D ERT data measured along river levees. The absence of water in the river results in more significant 3D effects. 3D effects approach the maximum of 30% for the monitored levee in San Giacomo. During the irrigation period, the presence of water in the canal reduces 3D effects to a maximum of about 15%. This was also observed in laboratory simulations, where 3D effects were maximum for dry period and minimum when the water level in the river side was higher.

The 3D effects for different input resistivity models of the levee (homogeneous and layered) showed similar trends, but the values were different for different models, even though the boundary conditions were similar. This shows that having a good knowledge of the material used for the construction of the levee is crucial to accurately quantify 3D effects. Moreover, variations of resistivity in the levee during different seasons should be considered when calculating 3D effects for each period. Samples obtained from the study site could improve synthetic models used for quantifying 3D effects. In the absence of a priori information about the levee material and granulometry variations with depth, an iterative approach can be suggested to improve 3D corrections progressively. An initial homogeneous model can be used to calculate preliminary 3D corrections. By inverting the data after preliminary corrections, a new non-homogeneous resistivity model is obtained and can be used to recalculate 3D corrections.

Our study also showed that the trend of 3D effects for the pilot site is not constant. As the electrode spacing is increased from the smallest values up to values roughly corresponding to depths equal to the bottom of the canal, 3D effects follow an increasing trend for all models. Further increase in electrode spacing results in a decreasing trend for 3D effects. This is due to significant concentration of current in the conductive soil for largest electrode spacings. For laboratory experiments, only an increasing trend was observed because the walls and the base of the flume are insulating boundaries.

The method discussed in this paper is beneficial for correcting ERT data to perform 2D inversions. The maximum difference in the apparent resistivity values calculated by directly adding the topography in 3D forward models and using the high resistivities to model the air was only about 0.2%, which is much less than the error in the measurements. The 3D effects can also be managed by defining correct boundary conditions for a 3D inversion, but a full 3D inversion requires much more computational time and memory. This is especially important in real-time monitoring where inverse models of daily (or more frequent) measured data sets are immediately generated.

Inversions of data after 3D corrections demonstrate that a 2D spread can be successfully used to monitor a critical segment of a levee producing reliable data that can be converted into water content maps. Reliable interpretations and quantitative water content maps are crucial to successfully employ ERT monitoring in early-warning alarm systems.

ACKNOWLEDGEMENTS

This research was partially funded by Fondazione Cariplo, Italy, grant number 2016-0785, and by Ministero dell'Ambiente e della Tutela del Territorio e del Mare, Italy, project DILEMMA – Imaging, Modeling, Monitoring and Design of Earthen Levees. We are grateful to Annachiara Fasulo, Matteo Eritrei, Federica Brambilla and Stefano Malorgio for their collaboration in laboratory activities. Annachiara Fasulo and Matteo Eritrei also helped in forward modelling of laboratory data in RES2DMOD and RES3DMODx64.

DATA AVAILABILITY STATEMENT

Data sets used in this research will be sent to interested researchers upon request.

ORCID

Azadeh Hojat https://orcid.org/0000-0002-1950-3607
Meng Heng Loke https://orcid.org/0000-0003-4935-8014

REFERENCES

Alfieri, L., Feyen, L., Dottori, F. and Bianchi, A. (2015) Ensemble flood risk assessment in Europe under high end climate scenarios. *Global Environmental Change*, 35, 199–212.

Arosio, D., Hojat, A., Ivanov, V.I., Loke, M.H., Longoni, L., Papini, M. *et al.* (2018) A laboratory experience to assess the 3D effects on 2D ERT monitoring of river levees. 24th European Meeting of Environmental and Engineering Geophysics, Porto. https://doi.org/10.3997/2214-4609.201802628.

Arosio, D., Munda, S., Tresoldi, G., Papini, M., Longoni, L. and Zanzi, L. (2017) A customized resistivity system for monitoring saturation and seepage in earthen levees: installation and validation. *Open Geosciences* 9, 457–467. https://doi.org/10.1515/geo-2017-0035.

Bièvre, G., Oxarango, L., Günther, T., Goutaland, D. and Massardi, M. (2018) Improvement of 2D ERT measurements conducted along a small earth-filled dyke using 3D topographic data and 3D computation of geometric factors. *Journal of Applied Geophysics*, 153, 100–112.

Chambers, J.E., Gunn, D.A., Wilkinson, P.B., Meldrum, P.I., Haslam, E., Holyoake, S. *et al.* (2014) 4D electrical resistivity tomography monitoring of soil moisture dynamics in an operational railway embankment, *Near Surface Geophysics*, 12, 61–72.

Chambers, J.E., Meldrum, P.I., Gunn, D.A., Wilkinson, P.B., Kuras, O., Weller, A.L. *et al.* (2009) Hydrogeophysical monitoring of landslide processes using automated time-lapse electrical resistivity tomography (ALERT). 15th European Meeting of Environmental and Engineering Geophysics.

Dahlin, T. (2000) Short note on electrode charge-up effects in DC resistivity data acquisition using multi-electrode arrays. *Geophysical Prospecting*, 48, 181–187.

Dahlin, T., Leroux, V., Larsson, R. and Rankka, K. (2005) Resistivity imaging for mapping of quick clays for landslide risk assessment. Near Surface 2005, Palermo, Italy.

Godio, A., Strobbia, C. and De Bacco, G. (2006) Geophysical characterisation of a rockslide in alpine region. *Engineering Geology*, 83, 273–286.

Heincke, B., Günther, T., Dalsegg, E., Rønning, J.S., Ganerød, J.V. and Elvebakk, H. (2010) Combined three-dimensional electric and seismic tomography study on the Åknes rockslide in western Norway. *Journal of Applied Geophysics*, 70, 292–306.

Hojat, A., Arosio, D., Ivanov, V.I., Longoni, L., Papini, M., Scaioni, M. *et al.* (2019a) Geoelectrical characterization and monitoring of slopes on a rainfall-triggered landslide simulator. *Journal of Applied Geophysics*, 170, 103844. https://doi.org/10.1016/j.jappgeo.2019.103844.

Hojat, A., Arosio, D., Loke, M.H., Longoni, L., Papini, M., Tresoldi, G. *et al.* (2019b) Assessment of 3D geometry effects on 2D ERT data of a permanent monitoring system along a river embankment. EAGE-GSM 2nd Asia Pacific Meeting on Near Surface Geoscience & Engineering, Kuala Lumpur, Malaysia. https://doi.org/10.3997/2214-4609.201900427.

Hojat, A., Arosio, D., Longoni, L., Papini, M., Tresoldi, G. and Zanzi, L. (2019c) Installation and validation of a customized resistivity system for permanent monitoring of a river embankment. EAGE-GSM 2nd Asia Pacific Meeting on Near Surface Geoscience & Engineering, Kuala Lumpur, Malaysia. https://doi.org/10.3997/2214-4609.201900421.

Hojat, A., Arosio, D., Di Luch, I., Ferrario, M., Ivanov, V.I., Longoni, L. *et al.* (2019d) Testing ERT and fiber optic techniques at the laboratory scale to monitor river levees. 25th European Meeting of Environmental and Engineering Geophysics, The Hague, Netherlands. https://doi.org/10.3997/2214-4609.201902440.

Karimi-Nasab, S., Hojat, A., Kamkar-Rouhani, A., Akbari-Javar, H. and Maknooni, S. (2011) Successful use of geoelectrical surveys in area no. 3 of the Gol-e-Gohar iron ore mine, Iran. *Journal of Mine Water and the Environment*, 30(3), 208–215. https://doi.org/10.1007/s10230-011-0135-7.

Kuras, O., Pritchard, J.D., Meldrum, P.I., Chambers, J.E., Wilkinson, P., Ogilvy, R.D. *et al.* (2009) Monitoring hydraulic processes with automated time-lapse electrical resistivity tomography (ALERT). *Comptes Rendus Geoscience*, 341(10), 868–885.

Loke, M.H. (2014) RES3DMODx64 ver. 3.04: 3-D resistivity and IP forward modeling using the finite-difference and finite-element methods. www.geotomosoft.com.

Loke, M.H. (2016) RES2DMOD ver. 3.03: rapid 2D resistivity and I.P. forward modeling using the finite-difference and finite-element methods. www.geotomosoft.com.

Loke, M.H. (2018) Rapid 2-D resistivity and IP inversion using the least-squares method. www.geotomosoft.com.

Menziani, M., Rivasi, M.R., Pugnaghi, S., Santangelo, R. and Vincenzi, S. (1996) Soil volumetric water content measurements using TDR technique. *Annali di Geofisica*, 39(1), 91–96.

Perrone, A., Lapenna, V. and Piscitelli, S. (2014) Electrical resistivity tomography technique for landslide investigation: a review. *Earth-Science Reviews*, 135, 65–82.

Piegari, E., Cataudella, V., Di Maio, R., Milano, L., Nicodemi, M. and Soldovieri, M.G. (2008) Electrical resistivity tomography and statistical analysis in landslide modelling: a conceptual approach. *Journal of Applied Geophysics*, 68(2), 151–158.

Rücker, C. and Günther, T. (2011) The simulation of finite ERT electrodes using the complete electrode model. *Geophysics*, 76(4), F227–F238. https://doi.org/10.1190/1.3581356.

Scaioni, M., Crippa, J., Yordanov, V., Longoni, L., Ivanov, V.I. and Papini, M. (2018) Some tools to support teaching photogrammetry for slope stability assessment and monitoring. *International Archives of the Photogrammetry, Remote Sensing and Spatial Information Sciences – ISPRS Archives*, 42(3W4), 453–460. https://doi.org/10.5194/isprs-archives-XLII-3-W4-453-2018.

Sjödahl, P., Dahlin, T. and Zhou, B. (2006) 2.5D resistivity modeling of embankment dams to assess influence from geometry and material properties. *Geophysics*, 71(3), G107–G114.

Supper, R., Ottowitz, D., Jochum, B., Kim, J.H., Romer, A., Baron, I. *et al*. (2014) Geoelectrical monitoring: an innovative method to supplement landslide surveillance and early warning. *Near Surface Geophysics*, 12(1), 133–150. https://doi.org/10.3997/1873-0604.2013060.

Telford, W.M., Geldart, L.P. and Sheriff, R.E. (1990) *Applied Geophysics*. Cambridge University Press, 770 p.

Tresoldi, G., Arosio, D., Hojat, A., Longoni, L., Papini, M. and Zanzi, L. (2018) Tech-levee-watch: experimenting an integrated geophysical system for stability assessment of levees. *Rendiconti Online della Società Geologica Italiana*, 46, 38–43. https://doi.org/10.3301/ROL.2018.49.

Tresoldi, G., Arosio, D., Hojat, A., Longoni, L., Papini, M. and Zanzi, L. (2019) Long-term hydrogeophysical monitoring of the internal condition of river levees. *Engineering Geology*, 259, 105139. https://doi.org/10.1016/j.enggeo.2019.05.016.

Uhlemann, S., Chambers, J., Falck, W.E., Alonso, A.T., Fernández González, J.L. and Espín de Gea, A.A. (2018) Applying electrical resistivity tomography in ornamental stone mining: challenges and solutions. *Minerals*, 8(11), 491. https://doi.org/10.3390/min8110491.

Uhlemann, S., Chambers, J., Wilkinson, P., Maurer, H., Merritt, A., Meldrum, P. *et al*. (2017) Four-dimensional imaging of moisture dynamics during landslide reactivation. *JGR Earth Surface*, 122, 1–21. https://doi.org/10.1002/2016JF003983.

Whiteley, J., Chambers, J.E. and Uhlemann, S. (2017) Integrated monitoring of an active landslide in Lias Group Mudrocks, North Yorkshire, UK. In: Hoyer, S. (Ed) GELMON 2017: 4th International Workshop on Geoelectrical Monitoring: Book of Abstracts, p. 27. www.iris-instruments.com/, last accessed on 20 November 2018.

Zhang, Z., Arosio, D., Hojat, A., Taruselli, M. and Zanzi, L. (2019) Construction of a 3D velocity model for microseismic event location on a monitored rock slope. EAGE-GSM 2nd Asia Pacific Meeting on Near Surface Geoscience & Engineering, Kuala Lumpur, Malaysia. https://doi.org/10.3997/2214-4609.201900382.

